Applied Physics A (2019) 125:432
https://doi.org/10.1007/s00339-019-2704-8

Applied Physics A
Materials Science & Processing

Comparison of the productivity and ablation efficiency of different laser classes for laser ablation of gold in water and air

Sarah Dittrich[1] · René Streubel[1] · Cormac McDonnell[2] · Heinz P. Huber[2] · Stephan Barcikowski[1] · Bilal Gökce[1]

Received: 11 January 2019 / Accepted: 8 May 2019 / Published online: 24 May 2019

Abstract
In this study, we compare different laser systems used for the synthesis of nanoparticles. The productivity and ablation efficiency of laser ablation of gold in water and in air are determined for three pulsed laser systems with comparable pulse energy but different pulse duration and repetition rate. All experiments are performed in a fluence range of up to 20 J/cm^2. The highest productivity among the considered lasers is found for a high-power picosecond laser, which shows 12 times higher ablation rate for the ablation in air compared to ablation in liquid. Further, we find that the threshold fluence for ablation in air is up to 1.9 times higher than for ablation in water. The highest ablation efficiency, which is defined as an energy specific ablation volume by the ablation rate divided by the laser power, is found for the low power, compact nanosecond laser system.

1 Introduction

Chemically synthesized colloids, e.g. those synthesized by the Turkevich method, are characterized by nanoparticles of defined size and monomodality [1]. However, disadvantages of chemically synthesized nanoparticles (NP) are residual precursors and reactant oxidation products in the colloid, which have negative effects on biological application, if they are not removed by post-processing steps such as washing of the colloid [2]. Purity is also important in the field of catalysis [3] and for analytical reference materials [4]. An alternative way to generate NP is by pulsed laser ablation in liquids (PLAL) since no additives or precursors are needed for this synthesis method [5]. Further advantages of PLAL include a broad variety of possible material–liquid combinations enabling the synthesis of unique and tailored colloids [6]. Moreover, the procedure is conceptually simple, reproducible and fast [7].

Accordingly, the applications of laser-synthesized nanoparticles span a wide area including catalysis [8, 9], magnetism [10–13], tribology [14] and additive manufacturing [15–18]. If PLAL should become a considerable alternative to the chemical synthesis of NP, the productivity of the process is crucial. Productivity is defined as the ablated mass per time and is given in [µg/s]. On the other hand, the efficiency of the process is described by the power-specific productivity. This is calculated by dividing the productivity by the power input and given in [mg/(Wh)]. Both expressions are used synonymously. This value has been suggested recently by Zhang et al., and Kohsakowski et al. [6, 19]. Both, the productivity and the power-specific productivity, can be influenced by the pulse duration, repetition rate, and pulse energy on the laser side and the energy per area on the target surface, pulse overlap, and scanning speed on the process side.

The lasers, chosen in this study, exhibit comparable pulse energy, but vary in the maximal power and in the laser pulse duration. The influence of the laser pulse duration on the mechanisms of laser–matter interaction has been discussed in the literature [20–22]. Also, empiric attempts to calculate the material removal rate by laser and ablation efficiency have been made with a simple model [23], where multiple laser pluses are applied on a target [20, 24–26]. However, a precise prediction is difficult because the simple model neglects the influence of certain factors. The model fit parameters, which are threshold fluence and effective penetration depth, are not described depending on, e.g. the pulse duration [27] and wavelength [28]. Consequently, the calculation of the removal rate depends on the considered laser system.

✉ Bilal Gökce
Bilal.Goekce@uni-due.de

[1] Technical Chemistry I and Center of Nanointegration Duisburg-Essen (CENIDE), University of Duisburg-Essen, Universitaetsstr. 7, 45141 Essen, Germany

[2] Lasercenter, Department 06, Munich University of Applied Sciences, Lothstr. 34, 80335 Munich, Germany

When comparing laser ablation in air with the ablation process in a liquid, the thermodynamic characteristics and kinetics of the mechanism change due to confinement by the liquid [29]. Though this has been known for many years, there are also recent findings explaining the interaction of the cavitation bubble with the surrounding liquid and nanoparticles [30] and the influence of the surrounding liquid on the ablation mechanism [31–34]. Most publications state a higher ablation rate in air [33, 35, 36]; Shaheen et al. [37], however, reported a higher ablation rate of brass in water, although they may have used fluences in the order of 100 J/cm^2 for their experiments, which is about a factor of 10–20 higher than the expected fluence for optimum ablation efficiency. Sajti et al. [38], on the other hand, compared ablation rates of $\alpha-Al_2O_3$ in air and water for different distances of consecutive laser pulses, pulse energies, and repetition rates, and found the ablation rate to be dependent on those parameters. Also, the laser pulse duration influences the ablation rate as shown for fs and ps lasers [39, 40]. Moreover, most of the theoretical consideration and calculations concerning the ablation rate, have been performed with regard to ablation in air [24, 25].

In this work, the parameters relevant for high productivities are studied by comparing three commercially available and well-established laser systems, representing three classes. The laser sources deliver comparable pulse energies in the range of 100 µJ at a near-infrared wavelength but exhibit different repetition rates, average output powers, and pulse durations. The mid-power laser system is one of the most commonly used laser types in PLAL, a diode-pumped Q-switched nanosecond (ns) laser providing an average maximal output power of 10 W and originally intended for laser cutting and marking in industry. The high-power laser in this comparison is a 500-W picosecond (ps) master oscillator power amplifier system (MOPA), comprising a mode-locked oscillator and a slab laser amplifier that demonstrated the highest productivity in laser ablation in liquid so far [41]. The low-power laser is a very compact passively Q-switched nanosecond laser, commonly named as micro-chip laser and usually used for spectroscopy, revealing the lowest average output power with 0.15 W.

When it comes to the use of nanoparticles in applications, it is important that with the chosen synthesis method (1) as many nanoparticles as possible can be produced with (2) as little energetic effort as possible. Hence, the first part of this paper presents the influence of the laser pulse duration on the productivity as well as the comparison of the ablation rate in water and in air for the different pulse durations. The second part describes the energetic consideration.

2 Methods and materials

2.1 Determination and comparison of the productivity of laser ablation for gold in water and air at different pulse durations

Two different ns lasers (Rofin Powerline E20 and CryLaS DSS1064-Q4) are compared with a ps laser (Amphos flex 500). The general data of the three laser systems are summarized in Table 1. The experimental setup and data for the comparison of the ablation in water and in air are given by Fig. 1 and Table 2.

Both ns lasers emit at 1064 nm but differ in pulse duration, maximal repetition rate, and maximal average power. The Rofin Powerline E20 (in the following referred to as "middle class" laser) is a CW diode-pumped, actively Q-switched $Nd:YVO_4$ laser in end-pumping configuration. It reaches a maximum average power of 10 W and a pulse duration of 5–10 ns, dependent on the laser power. The repetition rate can be adjusted up to 200 kHz and the maximum pulse energy of 403 ± 2 µJ is reached at a lower repetition rate. The CryLaS DSS1064-Q4 (in the following referred to as "compact class" laser) provides maximal pulse energy of 128 ± 1 µJ and a pulse duration of 1 ns. The latter is a passively Q-switched, diode-pumped micro-chip laser; therefore, the repetition rate of 1.2 kHz cannot be adjusted freely, but depends on the laser configuration and pump

Table 1 General parameters for the laser systems applied in this paper

Laser power class	Compact class	Middle class	High-end class
Laser name	CryLaS DSS-1064-Q4	Rofin Powerline E20	Amphos flex 500
Wavelength [nm]	1064	1064	1030
Pulse duration [ps]	1000	5000–10,000	3
Average maximal output power [W]	0.15	< 10	500
Repetition rate [Hz]	1–1200	$20–200 \times 10^3$	$(1.2–40.5)\times10^6$
M^2 [1]	< 1.4	< 1.5	< 1.2
Height × width × length of the ablation chamber [mm]	5 × 4 × 10	5 × 4 × 10	5 × 18 × 100
Time to scan the ablation area once [s]	0.3	0.3	0.06

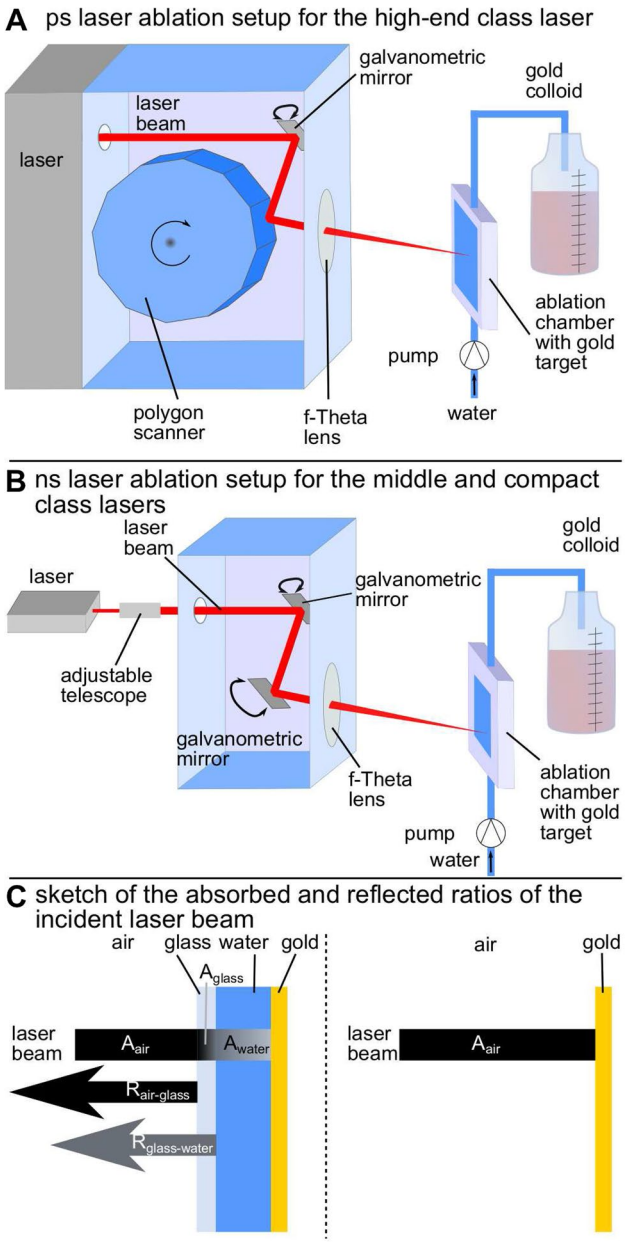

Fig. 1 Experimental setup for the high-end class (**a**) and the compact as well as the middle class (**b**) laser ablation, and a sketch illustrating the loss of laser energy for ablation in water and in air (**c**); the color gradient symbolizes the absorption A and the arrows the reflection R of the laser beam

power. Both lasers exhibit an almost TEM_{00} mode with an M^2 smaller than 1.5.

Since the laser beam diameter has an influence on the irradiated liquid volume and the beam diameter on the target surface, an adjustable telescope is used to set the diameter to approximately 4.4 mm, measured at $1/e^2$ intensity level. An f-Theta lens with a focal distance of 100 mm is used to focus the laser beam on the target surface. Before each experiment, the working distance is varied until the point of maximal productivity is found, which is considered as the distance of a maximum spot intensity and effective focal distance. All the following experiments are performed at this focal distance. The laser spot diameter on the target surface at the focal distance in water amounts to 61 ± 5 and 70 ± 6 µm for the CryLaS DSS1064-Q4 and the Rofin Powerline E20, respectively. The values are determined by measuring the spot diameter on the target surface. All ns laser experiments are performed in a liquid flow chamber at a flow rate of 5 mL/min and a repetition rate of 1.2 kHz. To place the laser pulses on separated spots on the sample to avoid laser beam shielding by the cavitation bubble, a nominal scan velocity of 10 m/s was selected, leading to a distance between the centers of two consecutive laser spots, also known as interpulse distance, of 8.3 mm, which is large compared to the spot diameter. It has to be mentioned that the same area is irradiated multiple times during the experiments to simulate conditions under long-term ablation. To vary the laser fluence, the average laser power is adjusted between 30 mW and the maximal laser power with an error of less than 1 % by measuring with a power meter (FieldMaxII-TOP, Coherent Inc.).

The ps MOPA laser system (in the following referred to as "high-end class" laser) provides a pulse duration of 3 ps and a maximal output power of 500 W. The high-end laser consists of a mode-locked ps oscillator, followed by a pulse-picker and slab laser crystal amplifier. The ps oscillator is operating at typically a few 10 MHz repetition rate at an average power of a few Watts leading to pulse energies of typically 100 nJ. The pulse-picker reduces the repetition rate of the seeder oscillator pulse train to 5000 kHz, before it is amplified to an average power of 500 W in the side-diode-pumped slab laser crystal corresponding to a pulse energy of 100 µJ. Because of the comparably high average output power and repetition rate, the flow rate is set to 510 mL/min and the effective scanning speed is increased to 484 m/s realized with a polygon scanner. This results in an interpulse distance on the sample surface of about 97 µm. The beam diameter on the target surface has an elliptical shape with the major and minor diameters of 148 ± 14 and 126 ± 7 µm, respectively. Thus, a pulse overlap of 35 % occurs on the target.

The material removal rates for the ablation in water for all three lasers are determined spectroscopically by UV–Vis extinction measurements. Since this is only applicable for nanoparticles with approximately the same size [42], a calibration for each laser was prepared by correlating the gold nanoparticles interband absorption at 380 nm with the gravimetrically determined mass productivity. In case of laser ablation in air, the material removal rate is determined gravimetrically after an ablation time of 5 min for both ns lasers and after 10 s for the high-end class laser. Each experiment

Table 2 Experimental parameter for the determination and comparison of the productivity of laser ablation in water and air for gold at different pulse durations

Laser power class	Compact class		Middle class		High-end class	
Ablation medium	Air	Water	Air	Water	Air	Water
Maximal absorbed fluence [J/cm^2]	5.5	6.3	17.4	21.0	2.3	1.3
Maximal pulse energy [µJ]	135	128	335	403	97	97
Spot diameter [µm]	79 ± 3	61 ± 5	70 ± 4	70 ± 6	120 ± 12; 86 ± 8	148 ± 14; 126 ± 7
Interpulse distance [µm]	8300	8300	8300	8300	79	79
Repetition rate [kHz]	1.2	1.2	1.2	1.2	5000	5000
Nominal scanning speed [m/s]	10	10	10	10	500	500
Flow rate [mL/min]	–	5	–	5	–	510
Flow velocity [cm/s]	–	0.4	–	0.4	–	9

Table 3 Values of the absorption (A) of the different media and the reflection (R) at the different layer interfaces, calculated by the Fresnel formula

	1064 nm	1030 nm
A_{air}	Neglected	Neglected
A_{water}	0.261	0.213
$R_{air\text{-}glass}$	0.041	0.041
$R_{glass\text{-}water}$	0.004	0.004

is carried out three times to calculate the average of the values and the standard deviation.

As shown by Streubel et al. [43] for liquid flow setups, the productivity stays constant with the ablation time and the quality of the colloid is not influenced, so that it is possible to extrapolate and compare the ablation rate. The focal distance is changed to the position of maximal productivity in air. Laser spot diameters on the target surface amount to 79 ± 3 and 70 ± 4 µm for the CryLaS DSS1064-Q4 laser and the Rofin Powerline E20 laser, respectively. For the Amphos flex 500 laser, an ellipse with major and minor diameters of 120 ± 12 and 86 ± 8 µm is determined.

For the data evaluation, the peak energy is converted to the laser peak fluence according to Eq. 1. To give a better comparison between laser ablation in air and in water, the reflection of the laser beam at the chamber entrance and absorption by water is considered (Fig. 1c). The reflection at the water–gold and air–gold interface is not taken into account because it has been reported in literature that a change in morphology lowers the reflectivity and increases energy absorption [44, 45]. The values of the absorption and reflectivity are given in Table 3 [46–48]. The values of the optical glass are taken from data sheets provided by SCHOTT North America, Inc.

The simple ablation model of Raciukaitis et al. [24] is given by Eq. 2, which requires the threshold fluence and the effective penetration depth to be fit. However, for a range of fluences between the threshold fluence and the optimal fluence, which equals the threshold fluence times e^2, also a linear plot can be applied, as an approximation. In this case, the threshold fluence can be determined as the intercept of the linear fit with the x-axis.

$$F_P = \frac{8 \times E_P}{\pi \times d^2}, \tag{1}$$

where F_P is peak fluence [J/cm^2], E_P peak energy [J], and d is spot diameter [µm].

$$\dot{m} = \frac{1}{16} \times f_R \times \pi \times \delta_{eff} \times d^2 \times \rho \times ln^2\left(\frac{F_P}{F_{th}}\right), \tag{2}$$

where $\dot{m}$ is productivity [µg/s], f_R repetition rate [1/s], δ_{eff} effective penetration depth [nm], ρ density [g/cm^3], and F_{th} is threshold fluence [J/cm^2].

2.2 Efficiency of laser ablation of gold in water

The laser power, repetition rate and distance between the ablation target and the focusing optics are varied to determine the point of maximal mass productivity. The final parameters are provided in Table 4. The parameters not mentioned in the table remain the same as described in Sect. 2.1 and given by Table 2. The experimental setup remains the same as depicted in Fig. 1. The resulting productivity of these experiments is divided by the average laser output power to calculate the power-specific productivity, or i.e. ablation efficiency in [mg/(Wh)], of the lasers.

3 Results and discussion

3.1 Determination and comparison of the productivity of laser ablation of gold in water and air at different pulse durations

In Fig. 2, the fluence-dependent productivity for gold in water for the high-end (Fig. 2a), compact (Fig. 2b), and

Table 4 Experimental parameter for determination of the maximal productivity and ablation efficiency of laser ablation of gold nanoparticles in water

Laser power class	Compact class	Middle class	High-end class
Pulse duration [ps]	1000	5000	3
Average laser output power [W]	0.15	5	500
Repetition rate [kHz]	1.2	15	5000
Pulse energy [µJ]	130	330	100
Maximal absorbed fluence [J/cm^2]	2.5	6.7	0.3
Interpulse distance [µm]	8300	670	97

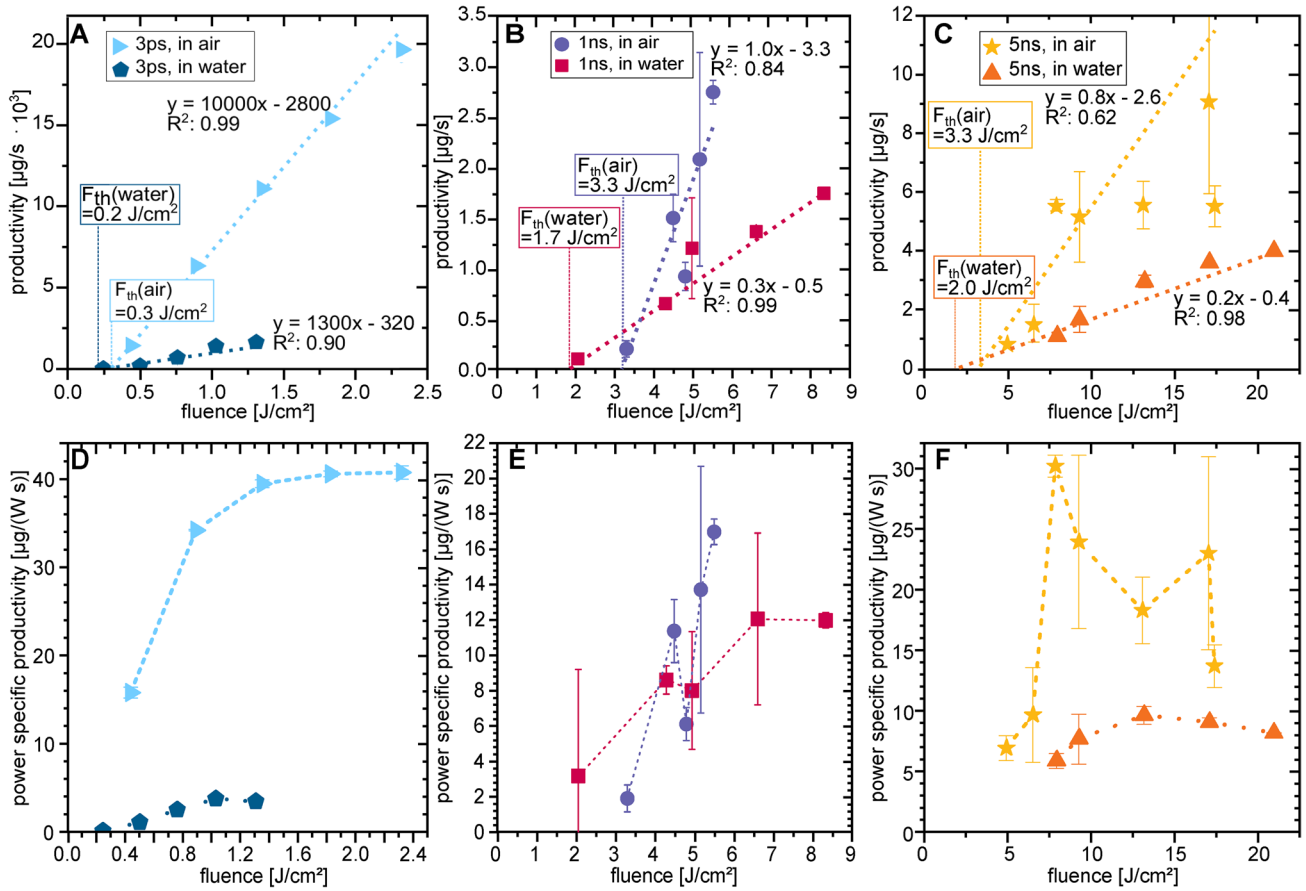

Fig. 2 The productivity for ablation in water and in air in dependency of the absorbed fluence for the high-end class laser (**a**), the compact class laser (**b**), and the middle class laser (**c**) is shown; the lines in **a**–**c** present the linear fit where the intercept with the *x*-axis marks the threshold fluence; the corresponding power-specific values of the same data are shown in **d**–**f**; in these cases, the lines connect the data point as a guide to the eye; error bars are included in all figures and represent the statistical error

middle (Fig. 2c) class lasers is presented. As expected, increasing the laser fluence leads to an increase in the productivity [41] for all lasers. Moreover, the high-end class laser provides the highest absolute productivity with nearly 1700 µg/s. Linear extrapolation from 10 s experiment to 1 h should be done with care, but would result in 6 g/h and is significantly higher than previously published for the same laser system (4 g/h) [41]. This deviation can be explained by an optimized focal position, a lowering of the pulse overlap from about 67 % to 35 % due to a lower repetition rate, and increased maximal pulse energy (from 50 to 100 µJ). The lowest productivity is reached with the compact laser class with 1.7 µg/s at about 8 J/cm^2, whereas the middle class reached maximal productivity at about 20 J/cm^2 (Fig. 2c).

According to Chichkov et al. [25], for a laser pulse duration τ_p smaller than a critical pulse duration required for electron–phonon equilibration, the threshold fluence remains independent of the laser pulse duration and is only a function of material properties. The critical pulse duration for gold is on the order of tens of ps. In the literature,

a value of 100 ps is often stated [49–51]. However, theoretical calculations of the threshold fluence in this regime are still difficult, since values for the reflectivity and the coefficient of absorption differ widely in literature [46, 52, 53]. Calculation of the threshold fluence is performed by measuring the crater diameter after single pulses, according to Gamaly et al., indicating a value of $0.5\,J/cm^2$ for gold in air [54, 55]. Saraeva et al. found ablation thresholds in water after single laser pulses for fs and ps lasers between 1 and $3\,J/cm^2$ [40]. For the high-end laser class, a threshold fluence of $0.2\,J/cm^2$ was found. One aspect which has to be considered is that most experiments in the literature are performed with a untreated surface. Vorobyev et al. [44] examined the influence of the surface morphology on the absorbed energy during laser ablation and found that a rough surface increases the absorbed energy to nearly 100 %. Scanning electron microscopy (SEM) images (Fig. 3) show a rough surface, which leads to the conclusion that also for ablation in water, a change in the surface morphology by previous pulses results in an increase in absorbed energy and consequently to a lower ablation threshold.

When increasing the pulse duration to the ns range, the electron and lattice temperature have time to reach equilibrium and electron heat conductivity plays the dominant role for heat diffusion. As the thermal penetration depth follows the well-known square-root dependence, the thermally affected volume also scales $\propto \sqrt{\tau_P}$. Thus, for the threshold fluence (F_{th}), a square root increase with pulse duration $\propto \sqrt{\tau_P}$ is expected in this regime, too [25, 56]. According to that, the expected increase in the threshold fluence from 1 ns to 5 ns should be a factor of approximately 2.2, whereas the experimental results (Fig. 2b) reveal only a change from 1.7 to $2.0\,J/cm^2$ in the threshold fluence for the compact and middle class lasers. However, this is theoretical and only based on a one-dimensional, two-temperature diffusion model [20]. In the model, energy loss due to heating perpendicular to the incident laser beam is neglected and also the interaction between the laser beam and the plasma plume is not taken into account. In literature, it has been reported that especially for laser pulses in the range of ns a portion of the laser beam energy is absorbed by the plasma [57]. Moreover, the amount of absorbed energy is higher for longer laser pulse durations [58]. Since this effect has not been studied systematically it is hardly possible to quantify the impact of the shielding by the plasma plume. Furthermore, plasma expansion increases for higher laser energies [59]. This means that the real absorbed laser fluence may be lower than calculated, leading to a shift of the fluence-graphs to lower fluences.

The highest power-specific ablation rate in water is determined for the compact class laser. This may be because for laser ablation in liquid not only the plasma but also the produced nanoparticles itself shield part of the laser beam [60]. The NP shielding effect is especially relevant for high repetition rates and high productivities, as gained with the high-end class laser. Due to the ultrahigh repetition rate with this laser, the a lateral pulse overlap is about 35 % and the temporal delay of successive laser pulses is 200 ns. A calculation of the flow velocity assuming laminar flow and using the values provided by Tables 1 and 2 within the ablation chamber for ablation in liquid results in 9 cm/s. This rough calculation reveals that the same fluid element, which contains NP, is hit by the laser more than 15 times while moving through the ablation chamber. The real flow behavior is determined by intermixing and diffusion, which leads to a higher mean residence time and more interaction of the fluid element with the laser beam. This calculation may be an explanation for the low ablation rate per pulse and energy input for the high-end class laser in water. During the compact and middle class laser experiments, no lateral

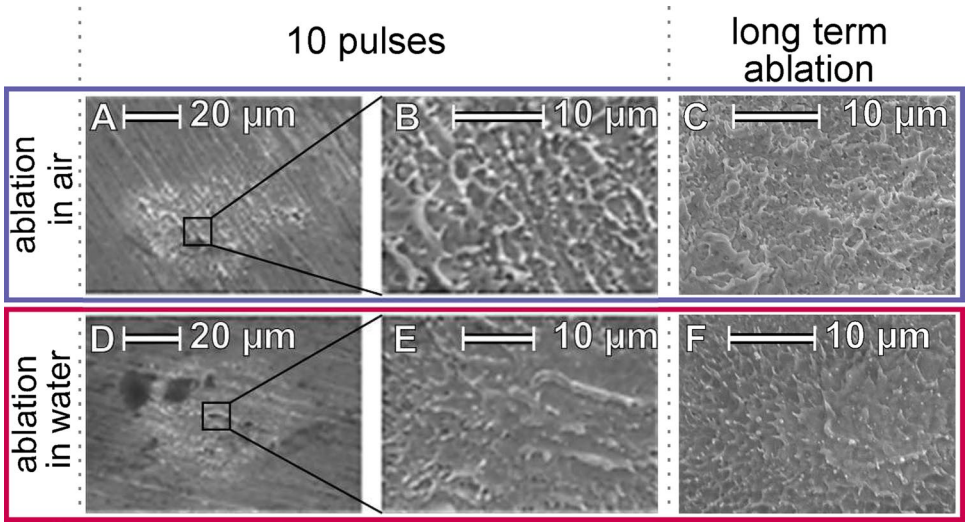

Fig. 3 SEM images of the ablated spot after ten pulses and after long-term ablation with the compact class laser are shown for ablation in air in **a–c** and ablation in water in **d–f**

and temporal pulse overlap occurs. Furthermore, lower NP concentrations were achieved in these experiments and the NP have an approximate mean residence time of three pulses in the ablation chamber, which significantly reduces the possibility of re-irradiation and consequently laser beam shielding. We assume that the laser shielding due to ablation products from the previous pulse is negligible.

The maximal productivity is considered to correspond to the maximal NP productivity. It has been shown in previous studies with the same laser systems and experimental conditions that gold nanoparticles synthesized in liquid are always smaller than 100 nm [43, 61]. However, it should be noted that if higher laser pulse durations (> 100 ns) are used to ablate metal targets in liquids, plasma-mediated melt expulsion is also possible, leading to even larger particles [62].

Although the absorption of the laser beam in the case of the ablation in water is considered in Fig. 2, a higher ablation rate is found for ablation in air. The highest increase by a factor of 10 for the comparison of ablation in water and in air is found for the high-end class laser.

When comparing the threshold fluences, the values for ablation in air are between 1.5 and 1.9 times higher for all laser systems. In the case of ablation with the middle class laser in air, the values should be considered with caution since the data points fluctuate strongly. Therefore, we only discuss the results qualitatively. Figure 3 shows SEM images of the gold surface in air and in water after ten pulses. Since the ablated area looks similarly rough in both cases, it is not possible to explain the lower ablation thresholds in water without further characterization.

The ablation efficiency in air and in water is shown in Fig. 2d–f. A drop in the power-specific productivity for fluences above e^2 times the threshold fluence as, for example, shown by Jaeggi et al. [63] cannot be seen in our data since the maximal possible laser power is reached at this point. Please recall in this context, that we measure the highest productivities for the described lasers. We do not claim to cover the whole range of fluences for the lasers classes.

The higher efficiency is found in air and the absolute highest efficiency is in case of the high-end laser class with more than 40 µg/(Ws). This value is about 11.0 times higher than for ablation with the same laser in water, whereby it increases by 1.4 and 2.4 for the compact and the middle class lasers, respectively. But it should also be considered, that for the compact and middle class lasers, the maximal levels reached in the experiments are more than 5 J/cm^2 lower than the optimal ablation fluence, which makes a comparison for all three lasers at that point difficult. This observation supports the hypothesis that effects reducing the energy input, such as the absorption and scattering by NP, particularly occur for the high-end class laser ablation in water, where high local NP concentrations are reached [64]. One reason for the strong increase in air for this laser class can be the difference in the ablation mechanism of ns compared to ps lasers. In the case of ablation in air, the ablation products, a mixture of vapor, atomic clusters, and droplets, are generated in a phase explosion of superheated metal and can propagate freely and rapidly away from the target. In a liquid water environment, the ablation plume is decelerated and a dense superheated molten metal layer is formed at the interface of ablation plume and water. Shih et al. simulated this for ps laser ablation of silver at 0.6 J/cm^2 [33, 65] and explained the lowering in the ablation rate per pulse and energy for the ablation in water. When comparing the ablation rate per pulse and energy input for the compact and middle class lasers, the increase from water to air is higher for the compact class laser, as already observed for the ablation in water. Since lower particle concentrations were obtained in the compact and middle class laser experiments, the shielding of the laser beam radiation by the particles is of minor importance. Moreover, the fluence for ablation with these two lasers in air is not high enough to reach the phase explosion regime.

3.2 Efficiency of laser ablation of gold in water

If the process of laser ablation in liquid should become a viable alternative to the colloids commercially available or the chemical synthesis of colloids [7], it is crucial for the ablation process to reach a high efficiency, i.e. power-specific productivity, and productivity. For the results in this section, laser power and repetition rate were varied to reach the point of maximal productivity, accessible within the given parameter range. The productivity for the middle class laser could be increased to about 10 µg/s (Fig. 4). Since the efficiency of the different laser systems should be discussed, the power-specific productivity is shown in Fig. 4b and the maximal values are compared in Fig. 4c and d. The maximum in the power-specific productivity was not reached, but the compared data points represent the efficiency at maximal productivity.

In literature, it has been stated that lasers with lower pulse duration, especially when comparing sub-ns to fs lasers, provide higher ablation rates [66]. This is indicated in Fig. 4c. As expected, the compact class laser providing the lowest average output power reached the lowest productivity (Fig. 4c) but the highest ablation efficiency (Fig. 4d). As previously discussed, it can be assumed that for the chosen parameters most of the ablated mass forms NP. With this assumption, it can be concluded that NP produced with the compact class are produced with the lowest average power input.

As can be seen in Fig. 4b all three laser systems (nearly) operate at the optimal fluence. As discussed in Sect. 3.1, different effects lower the efficiency of the high-end class laser. When comparing the results for the middle class laser

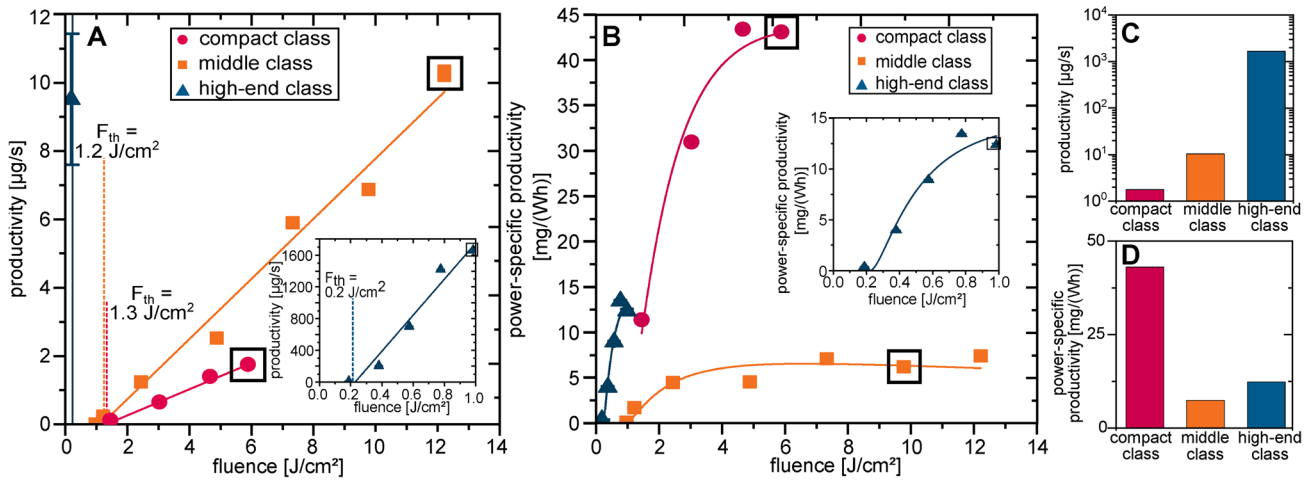

Fig. 4 Maximal fluence-dependent productivity for the three laser classes (**a**) and the corresponding fluence-dependent power-specific productivity (**b**), the maximal values for the productivity (**c**) and the power-specific productivity (**d**) are compared; the values used for **c** and **d** are marked with squares in **a** and **b**; the lines in **a** and **b** connect the data points as a guide to the eye; error bars are included in all figures and represent the statisticial error

system operating at lower (Fig. 2) and higher (Fig. 4a and b) absolute productivities, it can be seen that the experiments were performed in comparable fluence ranges and for both experiments, the value of optimal fluence was reached. When comparing the ablation efficiencies for both experiments, a lower value is found for the experiment with the higher absolute ablation rate, although no pulse overlap occurs in both experiments. It has been reported in literature [67, 68], that with high repetition rates a higher part of the laser beam energy is absorbed by the NP which is in agreement with the experimental results for the middle class laser.

4 Conclusion

The fluence-dependent productivity, threshold fluence, and ablation efficiency of PLAL of gold were determined for ablation in water and in air for three different laser power classes operating at different pulse durations. All experiments were performed in a fluence range of up to 20 J/cm^2. Although the reflection and absorption of the laser energy by the water were taken into account, the maximal ablation rate in air is higher than for ablation in water. This effect cannot be explained by a difference in the surface structure of the ablated targets. Partially, this effect can be correlated with shielding by the produced NP in the liquid environment. Also, shielding due to the plasma plume must be taken into account, especially for ns laser pulses. However, further investigations are needed to understand the higher ablation rate in air compared to ablation in water.

Furthermore, the threshold fluence for the ablation in water is lower compared to ablation in air. Effects such as changes in reflectivity and morphology do not explain this observation; therefore, further investigations are required.

When comparing the efficiency of the three different lasers operating at parameters providing the maximal absolute productivity in the chosen fluence range, the compact class laser system, providing only 0.15 W output power, reached the lowest absolute productivity but by far the highest ablation efficiency. It is assumed that the largest part of ablated mass results in NP formation. The shielding of the laser energy because of the higher repetition rate of the middle and high-end class lasers causes the drop in ablation efficiency. As a consequence, a high ablation efficiency is reached for a low repetition rate (1.2 kHz in our case) while reaching sufficient pulse energies.

Acknowledgements This work was financially supported by the BMWi via ZIM AIF project under Grant no. ZF4044504RE6 and the Deutsche Forschungsgemeinschaft (DFG) [grant numbers GO 2566/7-1, HU 1893/6-1]. The authors gratefully thank the CryLaS GmbH in Berlin for provision of the DSS1064-Q4 laser, Ruksan Nadarajah for providing the SEM images and Prof. L. Zhigilei for fruitful discussions.

References

1. J. Turkevich, P.C. Stevenson, J. Hillier, A study of the nucleation and growth processes in the synthesis of colloidal gold. Discuss. Faraday Soc. **11**, 55 (1951)
2. S.K. Balasubramanian, L. Yang, L.Y.L. Yung, C.N. Ong, W.Y. Ong, L.E. Yu, Characterization, purification, and stability of gold nanoparticles. Biomaterials **31**, 9023–9030 (2010)
3. S. Gu, J. Kaiser, G. Marzun, A. Ott, Y. Lu, M. Ballauff, A. Zaccone, S. Barcikowski, P. Wagener, Ligand-free gold nanoparticles as a reference material for kinetic modelling of catalytic reduction of 4-nitrophenol. Catal. Lett. **145**, 1105–1112 (2015)

4. V. Amendola, L. Litti, M. Meneghetti, LDI-MS assisted by chemical-free gold nanoparticles: enhanced sensitivity and reduced background in the low-mass region. Anal. Chem. **85**, 11747–11754 (2013)
5. S. Petersen, J. Jakobi, S. Barcikowski, In-situ bioconjugation—novel laser based approach to pure nanoparticle-conjugates. Appl. Surf. Sci. **255**, 5435–5438 (2009)
6. D. Zhang, B. Gökce, S. Barcikowski, Laser synthesis and processing of colloids: fundamentals and applications. Chem. Rev. **117**, 3990–4103 (2017)
7. S. Jendrzej, B. Gökce, M. Epple, S. Barcikowski, How size determines the value of gold—economic aspects of wet chemical and laser-based metal colloid synthesis. Chem. Phys. Phys. Chem. **18**, 1012–1019 (2017)
8. J. Zhang, M. Chaker, D. Ma, Pulsed laser ablation based synthesis of colloidal metal nanoparticles for catalytic applications. J Colloid Interface Sci. **489**, 138–149 (2017)
9. F. Davodi, E. Mühlhausen, M. Tavakkoli, J. Sainio, H. Jiang, B. Gökce, G. Marzun, T. Kallio, Catalyst support effect on the activity and durability of magnetic nanoparticles: toward design of advanced electrocatalyst for full water splitting. ACS Appl. Mater. Interfaces **10**, 31300–31311 (2018)
10. T. Schmitz, U. Wiedwald, C. Dubs, B. Gökce, Ultrasmall yttrium iron garnet nanoparticles with high coercivity at low temperature synthesized by laser ablation and fragmentation of pressed powders. ChemPhysChem **18**, 1125–1132 (2017)
11. S. Barcikowski, T. Baranowski, Y. Durmus, U. Wiedwald, B. Gökce, Solid solution magnetic FeNi nanostrand-polymer composites by connecting-coarsening assembly. J. Mater. Chem. C **3**, 10699–10704 (2015)
12. V. Amendola, P. Riello, M. Meneghetti, Magnetic nanoparticles of iron carbide, iron oxide, iron@iron oxide, and metal iron synthesized by laser ablation in organic solvents. J. Phys. Chem. C **115**, 5140–5146 (2011)
13. A. Kanitz, J.S. Hoppius, M. Del Mar Sanz, M. Maicas, A. Ostendorf, E.L. Gurevich, Synthesis of magnetic nanoparticles by ultrashort pulsed laser ablation of iron in different liquids. ChemPhysChem **18**, 1155–1164 (2017)
14. S. Jendrzej, L. Gondecki, J. Debus, H. Moldenhauer, P. Tenberge, S. Barcikowski, B. Gökce, Tribological properties of laser-generated hard ceramic particles in a gear drive contact. Appl. Surf. Sci. **467–468**, 811–818 (2019)
15. C. Doñate-Buendía, F. Frömel, M.B. Wilms, R. Streubel, J. Tenkamp, T. Hupfeld, M. Nachev, E. Gökce, A. Weisheit, S. Barcikowski, F. Walther, J.H. Schleifenbaum, B. Gökce, Oxide dispersion-strengthened alloys generated by laser metal deposition of laser-generated nanoparticle-metal powder composites. Mater. Design **154**, 360–369 (2018)
16. R. Streubel, M.B. Wilms, C. Doñate-Buendía, A. Weisheit, S. Barcikowski, J.H. Schleifenbaum, B. Gökce, Depositing laser-generated nanoparticles on powders for additive manufacturing of oxide dispersed strengthened alloy parts via laser metal deposition. Jpn. J. Appl. Phys. **57**, 040,310 (2018)
17. T. Hupfeld, T. Laumer, T. Stichel, T. Schuffenhauer, J. Heberle, M. Schmidt, S. Barcikowski, B. Gökce, A new approach to coat PA12 powders with laser-generated nanoparticles for selective laser sintering. Procedia CIRP **74**, 244–248 (2018)
18. M.B. Wilms, R. Streubel, F. Frömel, A. Weisheit, J. Tenkamp, F. Walther, S. Barcikowski, J.H. Schleifenbaum, B. Gökce, Laser additive manufacturing of oxide dispersion strengthened steels using laser-generated nanoparticle-metal composite powders. Procedia CIRP **74**, 196–200 (2018)
19. S. Kohsakowski, A. Santagata, M. Dell'Aglio, A. de Giacomo, S. Barcikowski, P. Wagener, B. Gökce, High productive and continuous nanoparticle fabrication by laser ablation of a wire-target in a liquid jet. Appl. Surf. Sci. **403**, 487–499 (2017)
20. B.N. Chichkov, C. Momma, S. Nolte, F. von Alvensleben, A. Tünnermann, Femtosecond, picosecond and nanosecond laser ablation of solids. Appl. Phys. A **63**, 109–115 (1996)
21. N.M. Bulgakova, A.V. Bulgakov, I.M. Bourakov, N.A. Bulgakova, Pulsed laser ablation of solids and critical phenomena. Appl. Surf. Sci. **197–198**, 96–99 (2002)
22. L.S. Brown, T.W.B. Kibble, Interaction of intense laser beams with electrons. Phys. Rev. **133**, A705–A719 (1964)
23. J. Furmanski, A.M. Rubenchik, M.D. Shirk, B.C. Stuart, Deterministic processing of alumina with ultrashort laser pulses. J. Appl. Phys. **102**, 073,112 (2007)
24. G. Raciukaitis, M. Brikas, P. Gecys, B. Voisiat, M. Gedvilas, Use of high repetition rate and high power lasers in microfabrication: how to keep the efficiency high? JLMN **4**, 186–191 (2009)
25. B.N. Chichkov, C. Momma, S. Nolte, F. von Alvensleben, A. Tünnermann, Ablation of metals by ultrashort laser pulses. J. Opt. Soc. Am. B **14**, 2716–2722 (1997)
26. S. Preuss, A. Demchuk, M. Stuke, Sub-picosecond UV laser ablation of metals. Appl. Phys. A Mater. Sci. Process. **61**, 33–37 (1995)
27. B. Neuenschwander, B. Jaeggi, M. Schmid, From fs to sub-ns: dependence of the material removal rate on the pulse duration for metals. Phys. Procedia **41**, 794–801 (2013)
28. N. Patra, K. Akash, S. Shiva, R. Gagrani, H.S.P. Rao, V.R. Anirudh, I.A. Palani, V. Singh, Parametric investigations on the influence of nano-second Nd^{3+}:YAG laser wavelength and fluence in synthesizing NiTi nano-particles using liquid assisted laser ablation technique. Appl. Surf. Sci. **366**, 104–111 (2016)
29. D. Devaux, R. Fabbro, L. Tollier, E. Bartnicki, Generation of shock waves by laser-induced plasma in confined geometry. J. Appl. Phys. **74**, 2268–2273 (1993)
30. C.Y. Shih, R. Streubel, J. Heberle, A. Letzel, M.V. Shugaev, C. Wu, M. Schmidt, B. Gökce, S. Barcikowski, L.V. Zhigilei, Two mechanisms of nanoparticle generation in picosecond laser ablation in liquids: the origin of the bimodal size distribution. Nanoscale **10**, 6900–6910 (2018)
31. S.I. Kudryashov, I.N. Saraeva, V.N. Lednev, S.M. Pershin, A.A. Rudenko, A.A. Ionin, Single-shot femtosecond laser ablation of gold surface in air and isopropyl alcohol. Appl. Phys. Lett. **112**, 203,101 (2018)
32. N.A. Inogamov, V.V. Zhakhovskii, V.A. Khokhlov, Dynamics of gold ablation into water. J. Exp. Theor. Phys. **127**, 79–106 (2018)
33. C.Y. Shih, C. Wu, M.V. Shugaev, L.V. Zhigilei, Atomistic modeling of nanoparticle generation in short pulse laser ablation of thin metal films in water. J. Colloid Interface Sci. **489**, 3–17 (2017)
34. M. DellAglio, R. Gaudiuso, O. de Pascale, A. de Giacomo, Mechanisms and processes of pulsed laser ablation in liquids during nanoparticle production. Appl. Surf. Sci. **348**, 4–9 (2015)
35. S. Barcikowski, A. Hahn, A.V. Kabashin, B.N. Chichkov, Properties of nanoparticles generated during femtosecond laser machining in air and water. Appl. Phys. A **87**, 47–55 (2007)
36. S.V. Starinskiy, Y.G. Shukhov, A.V. Bulgakov, Laser-induced damage thresholds of gold, silver and their alloys in air and water. Appl. Surf. Sci. **396**, 1765–1774 (2017)
37. M.E. Shaheen, J.E. Gagnon, B.J. Fryer, Femtosecond laser ablation of brass in air and liquid media. J. Appl. Phys. **113**, 213,106 (2013)
38. C.L. Sajti, R. Sattari, B. Chichkov, S. Barcikowski, Ablation efficiency of α-Al_2O_3 in liquid phase and ambient air by nanosecond laser irradiation. Appl. Phys. A Mater. Sci. Process. **100**, 203–206 (2010)
39. P.A. Danilov, A.A. Ionin, S.I. Kudryashov, A.A. Rudenko, I.N. Saraeva, D.A. Zayarny, Non-monotonic variation of Au nanoparticle yield during femtosecond/picosecond laser ablation in water. Laser Phys. Lett. **14**, 056,001 (2017)

40. I.N. Saraeva, S.I. Kudryashov, A.A. Rudenko, M.I. Zhilnikova, D.S. Ivanov, D.A. Zayarny, A.V. Simakin, A.A. Ionin, M.E. Garcia, Effect of fs/ps laser pulsewidth on ablation of metals and silicon in air and liquids, and on their nanoparticle yields. Appl. Surf. Sci. **470**, 1018–1034 (2019)
41. R. Streubel, S. Barcikowski, B. Gökce, Continuous multigram nanoparticle synthesis by high-power, high-repetition-rate ultrafast laser ablation in liquids. Opt. Lett. **41**, 1486–1489 (2016)
42. D.D. Evanoff, G. Chumanov, Synthesis and optical properties of silver nanoparticles and arrays. ChemPhysChem **6**, 1221–1231 (2005)
43. R. Streubel, G. Bendt, B. Gökce, Pilot-scale synthesis of metal nanoparticles by high-speed pulsed laser ablation in liquids. Nanotechnology **27**, 1–9 (2016)
44. A.Y. Vorobyev, C. Guo, Enhanced absorptance of gold following multipulse femtosecond laser ablation. Phys. Rev. B **72**, 1496 (2005)
45. S. Reich, A. Letzel, B. Gökce, A. Menzel, S. Barcikowski, A. Plech, Incubation effect of pre-irradiation on bubble formation and ablation in laser ablation in liquids. ChemPhysChem **20**, 1036–1043 (2019)
46. P.B. Johnson, R.W. Christy, Optical constants of the noble metals. Phys. Rev. B **6**, 4370–4379 (1972). https://doi.org/10.1103/PhysRevB.6.4370
47. G.M. Hale, M.R. Querry, Optical constants of water in the 200-nm to 200-microm wavelength region. Appl. Opt. **12**, 555–563 (1973)
48. P.E. Ciddor, Refractive index of air: new equations for the visible and near infrared. Appl. Opt. **35**, 1566–1573 (1996)
49. J. Hohlfeld, S.S. Wellershoff, J. Güdde, U. Conrad, V. Jähnke, E. Matthias, Electron and lattice dynamics following optical excitation of metals. Chem. Phys. **251**, 237–258 (2000)
50. R.R. Letfullin, T.F. George, G.C. Duree, B.M. Bollinger, Ultrashort laser pulse heating of nanoparticles: comparison of theoretical approaches. Adv. Opt. Technol. **2008**, 1–8 (2008)
51. S.S. Wellershoff, J. Hohlfeld, J. Güdde, E. Matthias, The role of electron–phonon coupling in femtosecond laser damage of metals. Appl. Phys. A Mater. Sci. Process. **69**, S99–S107 (1999)
52. K.M. McPeak, S.V. Jayanti, S.J.P. Kress, S. Meyer, S. Iotti, A. Rossinelli, D.J. Norris, Plasmonic films can easily be better: rules and recipes. ACS Photonics **2**, 326–333 (2015)
53. S. Babar, J.H. Weaver, Optical constants of Cu, Ag, and Au revisited. Appl. Opt. **54**, 477 (2015)
54. E.G. Gamaly, A.V. Rode, B. Luther-Davies, V.T. Tikhonchuk, Ablation of solids by femtosecond lasers: ablation mechanism and ablation thresholds for metals and dielectrics. Phys. Plasmas **9**, 949–957 (2002)
55. B.C. Stuart, M.D. Feit, S. Herman, A.M. Rubenchik, B.W. Shore, M.D. Perry, Optical ablation by high-power short-pulse lasers. J. Opt. Soc. Am. B **13**, 459 (1996)
56. D. Du, X. Liu, G. Korn, J. Squier, G. Mourou, Laser-induced breakdown by impact ionization in SiO_2 with pulse widths from 7 ns to 150 fs. Appl. Phys. Lett. **64**, 3071–3073 (1994)
57. G. Yang, Laser ablation in liquids: applications in the synthesis of nanocrystals. Progress Mater. Sci. **52**, 648–698 (2007)
58. P. Peyer, L. Berthe, R. Fabbro, A. Sollier, Experimental determination by PVDF and EMV techniques of shock amplitudes induced by 0.6–3 ns laser pulses in a confined regime with water. J. Phys. D Appl. Phys. **33**, 498–503 (2000)
59. K.K. Kim, M. Roy, H. Kwon, J.K. Song, S.M. Park, Laser ablation dynamics in liquid phase: the effects of magnetic field and electrolyte. J. Appl. Phys. **117**, 074,302 (2015)
60. X. Liu, M. Atwater, J. Wang, Q. Huo, Extinction coefficient of gold nanoparticles with different sizes and different capping ligands. Colloids Surf. B Biointerfaces **58**, 3–7 (2007)
61. M.R. Kalus, N. Baersch, R. Streubel, E. Gökce, S. Barcikowski, B. Gökce, How persistent microbubbles shield nanoparticle productivity in laser synthesis of colloids—quantification of their volume, dwell dynamics, and gas composition. Phys. Chem. Chem. Phys. **19**, 7112–7123 (2017)
62. S.I. Kudryashov, A.A. Nastulyavichus, A.K. Ivanova, N.A. Smirnov, R.A. Khmelnitskiy, A.A. Rudenko, I.N. Saraeva, E.R. Tolordava, A.Yu. Kharin, I.N. Zavestovskaya, Y.M. Romanova, D.A. Zayarny, A.A. Ionin, High-throughput laser generation of Si-nanoparticle based surface coatings for antibacterial applications. Appl. Surf. Sci. **470**, 825–831 (2019)
63. B. Jaeggi, S. Remund, R. Streubel, B. Gökce, S. Barcikowski, B. Neuenschwander, Laser micromachining of metals with ultrashort pulses: factors limiting the scale-up process. J. Laser Micro/Nanoeng. **12**, 3 (2017)
64. G.X. Chen, M.H. Hong, T.C. Chong, H.I. Elim, G.H. Ma, W. Ji, Preparation of carbon nanoparticles with strong optical limiting properties by laser ablation in water. J. Appl. Phys. **95**, 1455–1459 (2004)
65. C. Wu, M.S. Christensen, J.M. Savolainen, P. Balling, L.V. Zhigilei, Generation of subsurface voids and a nanocrystalline surface layer in femtosecond laser irradiation of a single-crystal Ag target. Phys. Rev. B **91**, 375 (2015)
66. B. Jaeggi, B. Neuenschwander, M. Schmid, M. Muralt, J. Zuercher, U. Hunziker, Influence of the pulse duration in the ps-regime on the ablation efficiency of metals. Phys. Procedia **12**, 164–171 (2011)
67. R. Sattari, Laser-based fragmentation of microparticles for nanoparticle generation. J. Laser Micro/Nanoeng. **3**, 100–105 (2008)
68. P.K. Baruah, A.K. Sharma, A. Khare, Effective control of particle size, surface plasmon resonance and stoichiometry of Cu@Cu_xO nanoparticles synthesized by laser ablation of Cu in distilled water. Opt. Laser Technol. **108**, 574–582 (2018)